Quantitative Morphodynamics of Endothelial Cells within Confluent Cultures in Response to Fluid Shear Stress

Peter Dieterich,* Maria Odenthal-Schnittler,† Christof Mrowietz,‡ Michael Krämer,† Ludger Sasse,† Hans Oberleithner,† and Hans-J. Schnittler†

*Rechenzentrum der Universität Würzburg, Am Hubland, 97074 Würzburg, Germany; †Institut für Physiologie, Westfälische Wilhelms-Universität Münster, 48149 Münster, Germany; and ‡Dresdner Institut für Herz und Kreislaufforschung, 01099 Dresden, Germany

ABSTRACT To evaluate shear stress-induced effects on cultured cells we have extended the mechanical setup of a multichannel in vitro rheological system and developed software allowing entire processing control and image data analysis. The values of cell motility, degree of orientation (alignment), and cell elongation were correlated as a function of time (*morphodynamics*). Collective and individual endothelial cells within confluent cultures displayed a shear stress-dependent characteristic phase behavior of the following time course: resting conditions (phase I), change of motility (phase II), onset of alignment (phase III), and finally cell elongation (phase IV). Especially cell motility was characterized by a randomized zigzag movement around mean trajectories (fluctuations) together with mean cell locomotion. Onset of shear stress caused a down-regulation of fluctuations of 30% within $<$10 min and simultaneously increased locomotion velocities preferring the flow direction (phase II). After a lag period of 10 to 20 min cells orientated in the direction of flow (phase III) without significant cell elongation, which finally occurs within hours (phase IV). These data provide first evidence that cells within confluent endothelial monolayers respond to shear stress with a characteristic phase behavior.

INTRODUCTION

Fluid shear stress generated by blood flow is a physiological stimulus that primarily acts on endothelial cells lining the inner surface of the cardiovascular system. Shear stress is involved in control of endothelium-dependent regulation of blood pressure, coagulation-anticoagulation balance, angiogenesis, organ perfusion, and apoptosis. In addition, laminar flow might also be anti-arteriosclerotic (Niebauer and Cooke, 1996; Papadaki and Eskin, 1997; Davies, 1997; Takahashi et al., 1997; Sato et al., 1999; Gonzalez and Kannewurf, 1998; Skalak and Price, 1996; Nilius et al., 1997; Davies et al., 1992; Dormandy, 1996; Dimmeler et al., 1996; Traub and Berk, 1998; Ueba et al., 1997). Apart from physiological modulations, there is evidence that shear stress plays a critical role in the development of vascular impairments such as arteriosclerosis and re-perfusion injury following hypoxia and ischemia (Soler et al., 1997; Al-Mehdi et al., 1998; Birk-Sorensen et al., 1998; Traub and Berk, 1998; Hudlicka, 1998; Skalak and Price, 1996; Roca et al., 1998). An initial event in the development of arteriosclerosis is the disturbance of endothelial cells by altered flow conditions. By using cell culture models it has been shown that turbulent flow causes endothelial cell turnover (Davies et al., 1986) and the presence of shear stress gradients triggers cell detachment followed by increased migration activity (Tardy et al., 1997).

Endothelial cells in vivo and in culture respond to shear stress with activation of intracellular signaling pathways, release of specific mediators, transcriptional activation, gene expression, and finally a morphological change from a polygonal to an elongated phenotype in the direction of flow (Davies, 1991, 1995; Takahashi et al., 1997; Davies et al., 1992; Ando and Kamiya, 1996; Busse and Fleming, 1995; Dewey et al., 1981; Langille and Adamson, 1981; Eskin et al., 1984; Girard and Nerem, 1993; Nerem, 1993; Malek and Izumo, 1995). Cell orientation and elongation are considered to be an adaptive process of endothelial cells to reduce the local mechanical load and in turn to protect the cells from hydrodynamic injury. Shear stress-induced alignment and elongation of endothelial cells within a confluent monolayer requires coordinated temporal and spatial regulations of cellular subdomains including cell-to-substrate and cell-to-cell junctions. The role of cell-to-substrate adhesion during cell migration has been elegantly addressed by several groups using individual nonconfluent cells of various origin (Lauffenburger and Horwitz, 1996; Asthagiri et al., 1999; Palecek et al., 1998, 1999; Sastry et al., 1999; Huttenlocher et al., 1995; Sheetz et al., 1998, 1999). However, information on subcellular regulations, especially with respect to cell motility and activities at the cell-to-cell junctions in confluent cultures, is largely missing. Although the influence of cell-to-cell junctions seems to be obvious to coordinate shape change, cell orientation, and migration in shear stress-exposed confluent cultures, this topic has not been addressed yet. Recently, first evidence of the coordinated activity of cell-to-cell junctions and integrins was shown by expressing integrins in myoblasts, leading to cessation of motile activity (Huttenlocher et al., 1998). Some aspects of subcellular activities and regulations with respect to morphological changes have been addressed un-

Received for publication 17 November 1999 and in final form 27 May 2000.

Address reprint requests to Hans-J. Schnittler, Institut für Physiologie, TU-Dresden, Fetscherstrasse 74, 01307 Dresden, Germany. Tel.: 49-351-458-6007; Fax: 49-351-5378; E-mail: Hans.Schnittler@mailbox.TU-Dresden.de.

0006-3495/00/09/1285/13 $2.00

der shear stress conditions. It was shown that shear stress causes translocation of cell organelles (Coan et al., 1993), reorganization of actin filaments (Franke et al., 1984), and focal contacts (Davies et al., 1994), and increased migration activity under wound healing conditions (Tardy et al., 1997; Ando et al., 1987). Furthermore, alignment and shape change are dependent upon intact microtubules and tyrosine kinase activity (Malek and Izumo, 1996). Maintenance of endothelial integrity under shear stress has been demonstrated to be dependent from actin filaments in individual (Wechezak et al., 1989) and in confluent cell cultures (Schnittler et al., 1993). Integrity under shear stress is also related to junction-associated proteins such as Ca^{2+}-dependent cadherins and catenins, but not to PECAM-1 (platelet endothelial cell adhesion molecule) (Schnittler et al., 1990, 1997).

Cellular dysfunction mediated by certain agents such as inhibitors or drugs and by experimental manipulations on cells in cell biology research can be uncovered and quantified under shear stress conditions, whereas their effects are often not observable under resting (no shear stress) culture conditions. The same holds true for quantification of cell adhesion features with respect to immobilized proteins (Schnittler et al., 1993, 1997; Franke et al., 1988; Wechezak et al., 1989, 1993; Yap et al., 1997, 1998). Thus, in addition to the importance of flow on endothelial cell biology, shear stress can also be used as a valuable tool in research. However, discovering shear stress-induced morphological effects requires detailed quantitative analyses to obtain reliable results, especially in cell cultures. Consequently, an experimental system is required that allows automated data acquisition, processing control, and data analysis.

With respect to the importance of shear stress on endothelial structure and function and its applicability in cell biology and drug research, we have further enhanced the mechanical setup and hardware of an easy-to-handle multichannel rheological in vitro system that is based on a formerly described cone-and-plate device. This system allows generation of defined levels of fluid shear stress on cultured cells (Schnittler et al., 1993). Especially, we have developed a novel software for automated process control, image acquisition, and time-resolved on-line analysis of images under experimental fluid shear stress. Image analysis permits the calculation of a wide variety of parameters that allow the differentiated and quantitative characterization of cell behavior, even at the subcellular level, under flow. By using the high time resolution capability and the ability to acquire and analyze large amount of data, we first examined the early response of endothelial cells with respect to cell motility, alignment and cell elongation after the onset of shear stress. We show that endothelial cells respond and adapt to shear stress in a complex heterogeneous and phase-like mode. In addition, the results on the dynamical behavior of endothelial cells pose requirements for the development of a mathematical (biophysical) model of endothelial cell adaptation to fluid shear stress. Such a model could be useful to disentangle the interplay of different components on a quantitative mathematical basis.

MATERIALS AND METHODS

Mechanical setup and software development

Basics of the rheological setup

The setup is based on a cone-and-plate system (Schnittler et al., 1993). Cells are cultured on the plate where a rotating cone placed above the cell layer produces well-defined homogenous levels of fluid shear stress (Fig. 1) which is, in the lowest order of mathematical approximation, independent of the radial distance (Dewey et al., 1981). It was further shown that fluid shear stress of 0–200 dyn/cm^2 generated in the described cone-and-plate setup is laminar and mainly oriented in a circular direction (Schnittler et al., 1993). A small characteristic radial secondary flow occurs that does not disturb the laminar flow and is used for medium exchange. This has been shown using a colored medium either spotted on the plate or injected during shear stress application (Schnittler et al., 1993). Thus, medium exchange can be performed continuously, ensuring medium substitution and oxygen supply (Schnittler et al., 1993). Integrity of the cell monolayer, observation of dividing cells, lack of intercellular gap formation, and changes of morphodynamic parameters after shear stress interruption clearly indicate that medium exchange is successfully working and that the cell system remains in the best condition.

Furthermore, the system is transparent, allowing the on-line observation of endothelial cells by phase contrast and epifluorescence microscopy. The setup has two main advantages: 1) cultured cells can be directly observed during shear stress exposure and 2) up to 12 individual cone plate chambers can be mounted on a revolving plate, allowing investigations of manipulated and control cells of the same passage at different levels of shear stress within the same period of time.

Advanced automated rheological in vitro system: mechanical setup, autofocus, and cone velocity control

To systematically examine the influence of shear stress on cultured cells, especially with respect to the time-dependent morphological changes (*morphodynamic behavior*), we completely rebuilt and automated the in vitro rheological system according to Schnittler et al. (1993) (Fig. 1). Individual chambers are mounted on a rotary positioning stage. The microscope is fixed on a linear positioning stage. Rotating the revolver stand and moving the microscope linearly allows observation of the arbitrary points within each chamber with a repeating accuracy of $3.3 \cdot 10^{-3\circ}$ (corresponding to $\sim$16 μm) of the rotary positioning and smaller than 1 μm for the linear stage.

Autofocusing of the cell layer is realized by exploiting the properties of Fourier transformation of the microscopic phase contrast image in combination with a stepper motor. In contrast to a blurred image, a sharp image has a Fourier spectrum with the high frequencies necessary to resolve details.

The angular velocities of each head are controlled independently and, in addition, allow the generation of time-dependent shear stress profiles including pulsations up to 2 Hz. The process control implementation is based on the visual programming language LabVIEW (National Instruments, München, Germany). The program also accomplishes data acquisition and image segmentation and analysis.

Image processing pipeline

The image processing pipeline (Fig. 2) delivers segmentations of the cells consisting of the cell nucleus and perinuclear organelles as shown in Fig.

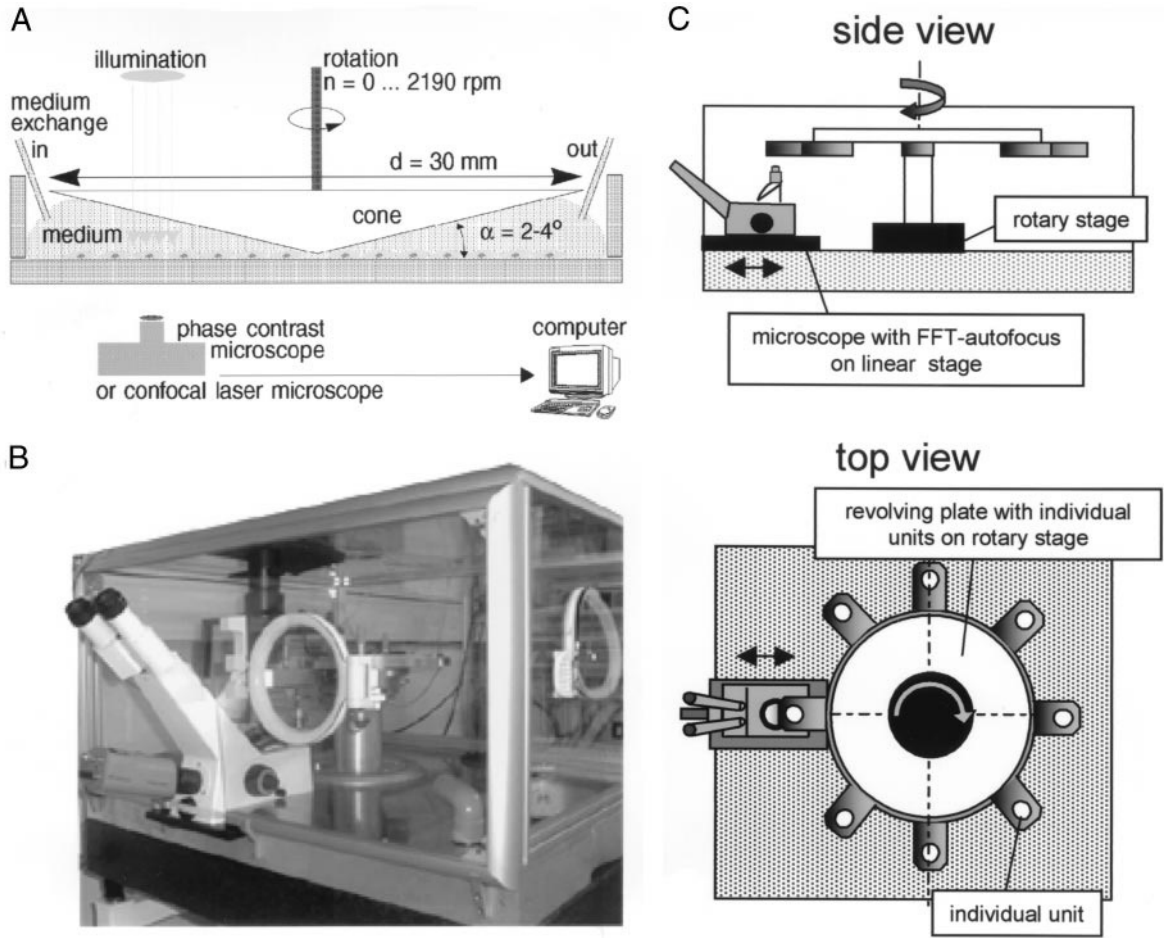

FIGURE 1 Mechanical setup of the automated rheological in vitro system. (*A*) Scheme illustrating the cone and plate device of one individual unit. (*B*) Overview of the total system, which is placed in an incubator. (*C*) Scheme explaining the arrangement of individual units on a revolver plate that is fixed on a rotary stage. The microscope is mounted on a linear stage. Rotating the revolver plate and moving the microscope linearly back and forward allows the observation of arbitrary points within each individual unit. Thus, arbitrary observations within each unit can be repeatedly performed.

2 (*lower segmented image*). Segmented areas typically have an area of ~50% related to the total cell area of confluent cell cultures (data not shown). Thus, the main parts of cells are included in the analyses of morphodynamics described later. We would like to point out that the described phenomena are restricted to these segments and do not directly include subcellular phenomena that occur exclusively at the cell borders. Segments directly deliver the position of each cell x_i and y_i (i.e., the center of mass of the segmentations), orientation φ_i (derived from the inertia tensor), area A_i, and perimeter P_i ($i = 1 \ldots N$, with N as the total number of cells within one image). Further quantifications can be derived from the generic data described in detail (see Applications and Results).

The image processing pipeline (Fig. 2) allows access to cell parameters described above. The implementation is based on IMAQ, an image processing extension of LabVIEW. The pipeline first corrects inhomogeneous illumination arising from the cone-plate geometry. Each image of 640 × 480 pixels (8-bit gray levels) is divided into 16 × 12 parts. These subimages are histogram-equalized, smoothed, and put together. Afterward, a threshold is set by a histogram-based technique. Small particles and cells touching the image boundaries are removed by morphological operations. Although there exist more sophisticated techniques of segmentation (Russ, 1999), this simple approach has proven to be robust and efficient, allowing one complete image processing run within <5 s per image on a simple 200 MHz personal computer. The resulting raw binary data set (consisting of cell positions, orientations, perimeters, and areas for all images) can be further used for postprocessing to calculate more sophisticated parameters such as correlation functions and cell motility parameters.

Segmentation and cell orientation

Endothelial cells display a flat morphology with an increase in cell height where the nucleus is located. The applied segmentation visualizes the cell nucleus and most of the nearby cellular organelles, such as the Golgi apparatus (GA) and endoplasmic reticulum. In confluent cell cultures, the real cellular boundaries are hardly accessible by phase contrast microscopy. Although ~50% of the culture surface is included in the morphodynamic analyses, we additionally investigated whether the long axes of the segmented areas represent the long axes of the total cell. Phase contrast images of endothelial cells were acquired and the cell-to-cell junctions of endothelial cells were subsequently stained by $AgNO_3$. Images were taken from areas formerly analyzed and long cell axes were determined by image analysis and related to long cell axes determined from cell boundaries. Overlaying $AgNO_3$-stained cell boundaries and segmentations based on phase contrast images of the very same cells displayed that long axes of the segmented areas largely fit the long axes of the total cell (Fig. 3). These results show that segmentation of endothelial cells by phase contrast microscopy is representative for long cell axes in confluent cultures of endothelial cells.

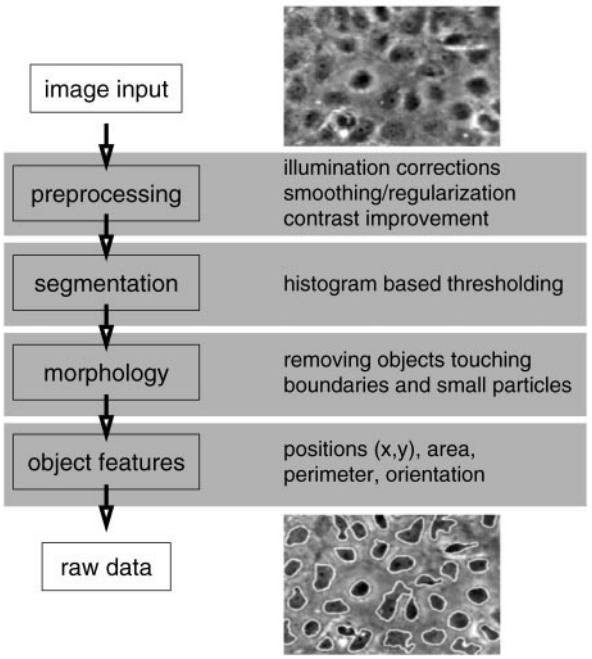

FIGURE 2 Illustration of the applied image processing pipeline. This procedure is applied to a series of images to calculate the positions, areas, orientations, and perimeters of cells within one image, e.g., at one time point. As an example, a part of an input image (*top*) is shown together with the segmented outlines (*bottom*).

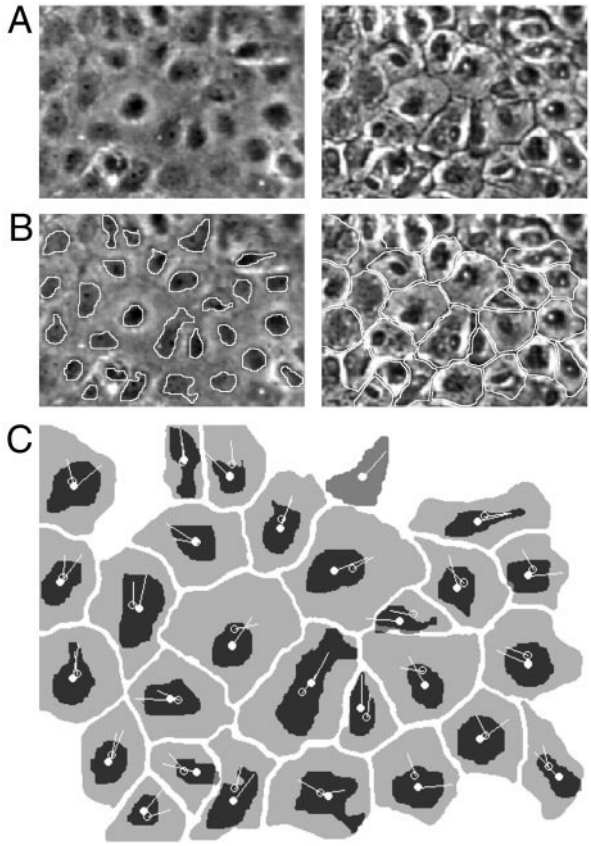

FIGURE 3 Comparison of cell orientations resulting from cell segments and real cell boundaries. A phase contrast image of living cells (*A*, *left*) was segmented applying the image processing procedure shown in Fig. 2; resulting cell segments are displayed (*B*, *left image*). Same cells were fixed and cell borders were stained by silver nitrate (*A*, *right image*) visualizing cell borders (*B*, *right image*). The results of *B* were used to calculate and compare the orientations of both types of cell contours. Image *C* shows the overlay of the resulting orientations, indicated by lines, by which filled circles denote cell centers obtained from phase contrast segments, whereas empty circles mark cell centers derived from silver nitrate-stained cell boundaries. Note cell axes largely display the same directions. Differences in orientations mainly occur for nearly round cells whose orientations are not clearly defined.

Cell culture

Pulmonary trunk endothelial cells were collected and cultured as described previously (Schnittler et al., 1990). Briefly, cells were cultured in Medium 199 supplemented with 10% fetal calf serum, 50 μg/ml streptomycin sulfate, and 50 U/ml penicillin G (Sigma, Deisenhofen, Germany). Cells were seeded on perfectly plane parallel round glass slides especially produced for rheological experiments previously coated with cross-linked gelatin as described elsewhere (Schnittler et al., 1993). For shear stress experiments the culture medium was used supplemented with 3% polyvinylpyrrolidone, MW 360,000 (Sigma, Deisenhofen, Germany) to increase the medium viscosity as described elsewhere (Schnittler et al., 1993).

Silver nitrate staining

Cell borders of cultured endothelial cells were visualized by silver nitrate staining. Therefore, cultures were rinsed briefly with distilled water (4°C) and then exposed for 10 min to 0.5% $AgNO_3$ dissolved in distilled water. Subsequently, cultures were rinsed three times for 1 min with distilled water and then (still covered with a thin layer of water) exposed to UV light for 5 min. This treatment clearly visualized the cell borders.

APPLICATIONS AND RESULTS

Morphodynamics of endothelial cells in response to fluid shear stress

By using the advanced facilities of the new system, we have studied in detail the response of cultured porcine endothelial cells to experimental fluid shear stress with high time resolution. In a first series of experiments we analyzed the dynamic behavior of morphological changes (*morphodynamics)* of confluent endothelial cells under fluid shear stress with respect to 1) cell motility, 2) flow-induced alignment, 3) cell elongation, and 4) the time relational changes to each other. To obtain accurate motility data, the corresponding experiments were performed with fixed positions of both the rotational and linear stages.

Individual cell paths within confluent cell cultures

Whereas the cell parameters at each time point available from the image processing pipeline can be used to calculate mean values (e.g., of orientations at time *t*), information is

missing about the behavior of individual cells within a confluent monolayer as a function of time. This knowledge is essential especially for confluent cultures to find phenomena and mechanisms leading to a better understanding of the internal cell dynamics. Thus, we have analyzed mean values and the behavior of individual cells of certain parameters to characterize shear stress-induced cell dynamics in confluent endothelial monolayers.

For this purpose a software tool was developed, which is able to derive individual cell paths from the data of the image processing pipeline. Within these primary raw data (compare Fig. 2), cell positions between different times are not related to each other, e.g., traces of individual cells are not available. Therefore, we have developed and implemented an algorithm (schematically illustrated in Fig. 4) which takes a cell position from the first image and looks for the corresponding cell at the next time step. The correct corresponding cell is defined as the cell with the smallest distance to the cell in question at the previous time point. The time interval between two successive images is so brief that the mean distance of cell movement within this time interval is much smaller than the mean cell-cell distance. A spatial cutoff was set for the correspondence if one-quarter of the mean cell-cell distance is exceeded. Consequently, the algorithm finds the trace of a single cell through the matrix of raw data (Fig. 4). A cell path ends at the last time point of the experiment or if the correspondence at some time cannot be achieved. This is done successively for all starting positions (each cell), until all raw data are analyzed. As a result of the described algorithm, individual cell paths and corresponding parameters are available as a function of time for every cell within the monolayer. Fig. 5 *A* gives a survey of found cell paths of a characteristic experiment together with the original images 20 min before and 60 min after the onset of shear stress ($t = 0$ min, 50 dyn/cm^2). A preferred locomotion of cells in the direction of flow is obvious, but a heterogeneity of individual cells can also be observed.

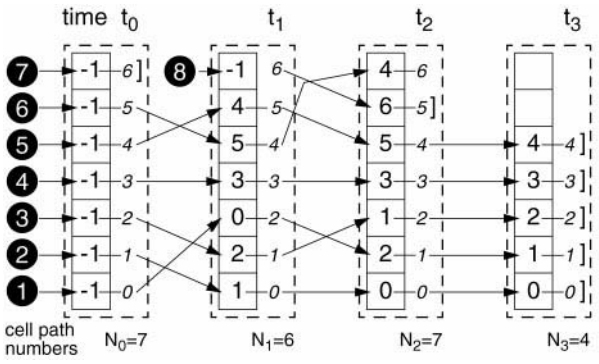

FIGURE 4 Schematic illustration of the cell trace algorithm that is able to find individual cell paths as a function of time. Each block (*dashed boxes*) at time t_i represents the numbered cells 0, 1, $\cdots$, ($N_i - 1$) (*right column*) resulting from the image processing pipeline. The numbers in boxes (*left column of dashed boxes*) denote the numbers of corresponding cells of the previous time step t_{i-1} (*numbers in boxes, left side*). The related cell is found by the distance criteria described in the text, where missing corresponding cells are marked with -1. The algorithm starts at time t_o and cell path number 1 (starting points of cell paths are marked with black circles). As an example, the first cell path is denoted by the cell numbers (0, 2, 1, 1). The final point of each path is marked with "]." The algorithm continues until all cells within the above matrix are exhausted. For the given example eight different paths are found.

To get more detailed information on this heterogeneity we have selected five individual cells (Fig. 5, *A* and *B*) which are representative for the cell ensemble. A rough classification of cells with respect to different qualitative and quantitative responses was performed delivering the criteria for the selection of these five individual cells. Obviously there are some cells responding with high locomotion over the substrate, such as cells 51 and 148 (faster than 51) and moving in the direction of shear stress. By contrast, cells 48 and 79 do not move directly in the direction of flow and show a relatively high lateral motility even in the presence of shear stress. Cell 8, however, shows a change in the migrational direction after the onset of shear stress. It is clear that there are some cells displaying different patterns, but these criteria hold roughly true for most of investigated cells.

As shown at higher resolution (Fig. 5 *B*), under resting conditions cell paths are randomly distributed, whereas under shear stress conditions (50 dyn/cm^2) the trajectories tend to be parallel to the direction of flow. Interestingly, within this flow-orientated trend cells frequently change their direction and even move orthogonal to the direction of flow (e.g., cells 48, 79, and 8 of Fig. 5 *B*). These individual cells were in particular analyzed with respect to further morphodynamic parameters (see below).

Analysis of motility

Within a confluent endothelial monolayer cell motility is a complex phenomenon that is influenced by internal and external (cell-to-substrate, cell-cell interactions) forces. The time lapse series of our experiments (Fig. 5) imply a shear stress-induced change in cell motility that can be decomposed in a directed locomotion over the substrate and fluctuations describing a zigzag movement of cells around mean trajectories (compare fine points in Fig. 5 *B*). Therefore, we examined the cell motility from different points of view: 1) spatial positions of individual cells as a function of time, 2) mean collective locomotion over the culture substrate, and 3) spatial fluctuations of cells around the mean cell path. Parameters were determined in the absence and presence of shear stress.

To find reliable calculations of cell velocities we have analyzed the development of cell positions x and y as a function of time. Fig. 6 displays the analyses of five different cells already shown in Fig. 5. Cell positions show fast fluctuations with time. Thus, a direct calculation of cell

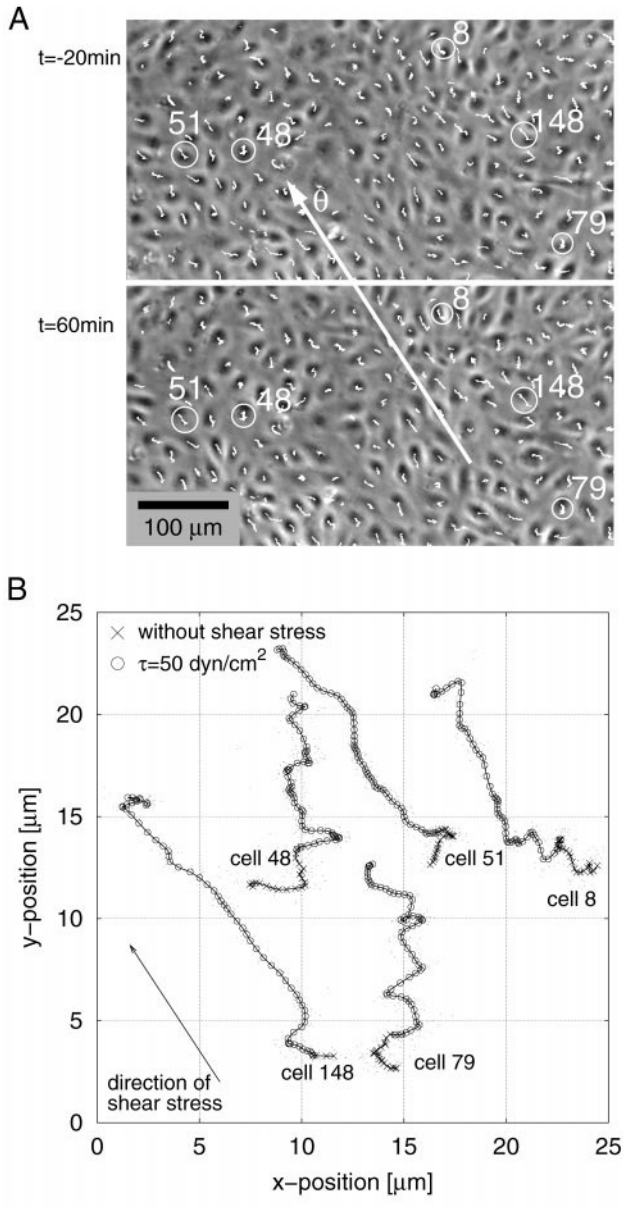

FIGURE 5 Cell trajectories. (*A*) Phase contrast images under resting conditions 20 min before onset of shear stress ($t = -20$ min) and at the end of the experiment ($t = 60$ min) after a 60-min shear stress exposure (starting at $t = 0$ min with a load of 50 dyn/cm^2 in θ-direction). The white lines in both images mark individual cell paths resulting form the cell trace algorithm (compare Fig. 4). Note, nearly all cells display trajectories. (*B*) Five representative cell trajectories (marked in *a* by circles) are displayed with higher resolution. Crosses denote the movement before the onset of shear stress (over a time interval of ~20 min), whereas circles represent the paths under the influence of shear stress. There is a time difference of 1 min between successive circles (or crosses). Fine points mark the measured positions of the cell centers, whereas the continuous lines together with circles and crosses represent mean trajectories as described in the text. Note the distances between circles are obviously larger than between crosses, indicating higher locomotion under shear stress. Also, distances of the measured points (*fine points*) are closer to the mean trajectories under shear stress than under resting conditions. Cells not displaying trajectories escaped the image analyses as described in the text. These cells are not included in the statistical analyses.

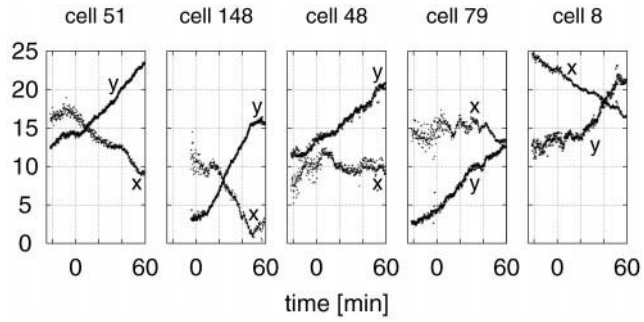

FIGURE 6 Individual cell movement. The cell coordinates x and y (given in μm) vary as function of time. Displayed are the same cells as in Figs. 5 and 9. The onset of shear stress starts at $t = 0$ min with a value of 50 dyn/cm^2. The following can be realized: cell 51 and cell 148 display obvious slope changes of both x- and y-coordinates within a few minutes after the onset of shear stress. The x- and y-slopes are greater for cell 148. Both slopes of cell 51 maintain their values during shear stress exposure, whereas the slopes of cell 148 again change their direction after 50 min. Also, the delay time differs between the two cells. Cell 48 does not obviously display a change in slope after the onset of shear stress. Cells 79 and 8, however, show a heterogeneity between slopes of the x- and y-coordinate, respectively. Where a change of slope of the y-coordinate can be observed of both cells, the slope of x-coordinate remains constant for cell 8. In addition, cell 79 undergoes a cyclic change. Importantly, cells react partly with a delay of some minutes to this change. Summarizing, cell locomotion given by the mean slope of curve changes in response to shear stress. Cells react heterogeneously and partly with delay.

velocity as differential quotient $\Delta x/\Delta t$ and $\Delta y/\Delta t$ would be mainly affected by these fluctuations and be extremely dependent on the choice of the time interval Δt.

Based on these considerations we calculated the mean trajectories according to

$$\bar{x}(t) = \frac{1}{\sqrt{2\pi}} \int_{t-T}^{t+T} x(t') \exp\left[-\frac{1}{2}\left(\frac{t' - t}{\Pi}\right)^2 \right] dt'$$

(and $y(t)$ analogously) which represents a Gaussian mean with width $\Pi = 2$ min and $T = 4$ min. Mean velocities are available as a gradient of the mean trajectories. Cells in Fig. 6 show a rather different motility behavior. Whereas cell 51 reacts nearly instantaneously to the onset of shear stress, cell 148 responds with a delay of ~15 min. Even the y-position of cell 48 shows this delay. However, the mean locomotion of most cells (on hand as mean slope of curves in Fig. 6) is enhanced by shear stress, typically after a time delay. This is clearly indicated by slopes of x and y in Fig. 6.

We further analyzed the mean locomotion velocities (v) and migration directions (ψ) of cell ensembles shown in Fig. 7 by a gray value plot of normalized probabilities $\rho(v)$ and $\rho(\psi)$ calculated from histogram distributions as a function of time. Both the first and the second onset of shear stress qualitatively display an increase of mean velocities v (Fig. 7 *A*, indicated by an extended distribution $\rho(v)$ toward higher v values) and a preferred direction of migration ψ parallel to the direction of flow θ (Fig. 7 *B*, as dark area around θ).

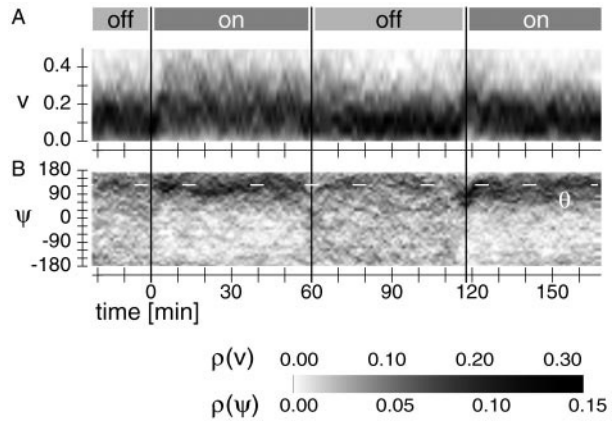

FIGURE 7 Onset and cessation of shear stress causes changes in mean velocities and orientations. Shear stress of 50 dyn/cm^2 was applied and interrupted to cultured endothelial cells as indicated (on/off). The same cells as in Fig. 5 were analyzed. Figures show gray value representations of normalized probability distributions ρ derived from histogram sampling as function of time. High probabilities are shown in dark colors, whereas low probabilities are lighter (details are given by the gray value map). (*A*) Gray values represent the distribution $\rho(v)$ of the mean cell velocities v. The onset of shear stress at $t = 0$ min causes (with a delay) the extension of velocities v to higher values. Interruption of shear stress at $t = 60$ min triggers a significant reduction. A second onset of shear stress at $t = 118$ min increased the mean velocities. (*B*) Gray values $\rho(\psi)$ display the probability distributions of mean directions of cell movements ψ. As seen for the velocities, onset of shear stress causes a mean directed cell movement parallel to the shear stress direction of $\theta = 123°$ that was absent under resting conditions or after shear stress interruption. Note changes in velocities and orientations are smaller after the second onset of shear stress compared to the first one.

Cessation of shear stress after 60 min causes a readjustment toward control levels after a delayed period of ~15–20 min for both parameters. The second onset, however, caused a reduced answer. In addition, the localization of $\rho(\psi)$ is relatively broad under shear stress, showing that not all cells move parallel to the direction of flow (Fig. 7 *B*). Finally, Fig. 7 *A* indicates the response delay to the onset of shear stress for the mean cell velocities that was observed for individual cells before.

In addition, Figs. 5 and 6 display spatial fluctuations of cell positions around their mean trajectories. These fluctuations (ξ) can be quantified as

$$\xi(t) = (\xi_x^2 + \xi_y^2)^{1/2}$$

with

$$\xi_x^2(t) = \frac{1}{2\delta}\int_{t-\delta}^{t+\delta} (x(t') - \bar{x}(t'))^2 \, dt'$$

and $\xi_{y,}$ analogously. These fluctuations are composed of measurement errors and real movements of the cell center. The measurement error consists of the finite pixel resolution and of changes in illumination mainly due to internal camera mechanisms. Whereas measurement errors due to finite pixel resolution are estimated theoretically as ~0.1 μm calculated for a 20× objective, the effect of illumination changes might be larger. To estimate these errors we have experimentally determined morphodynamic parameters on living cells under resting and shear stress conditions, and after fixation with 4% formaldehyde. Formaldehyde fixation abolishes real cell movements, but system-induced (artificial) experimental errors will be seen.

Whereas in this control experiment living cells showed fluctuations of ~0.2 μm around their mean trajectories, fixed cells displayed fluctuations only a few percent above the theoretical limit of 0.1 μm. Thus, spatial fluctuations of living cells are above the scatter of our setup evaluated by the analysis of fixed cells.

Fluctuations around the mean trajectories were compared with respect to the onset of shear stress. Fig. 8 *A* shows the spatial fluctuations of individual cells (compare Fig. 5) calculated within a time interval $\delta = 4$ min. At the onset of shear stress at $t = 0$ min, ξ clearly decreases. These data indicate a reduction of small zigzag movements of the center of cells. This is even confirmed for the mean fluctuations of all cells in Fig. 8 *B*. In addition, two points are remarkable: first, the decay of ξ takes place in ~10 min. However, the time interval is only an upper limit due to the averaging definition of ξ. The real decay time might even be below. Second, we have observed this reduction for different cell densities and levels of shear stress.

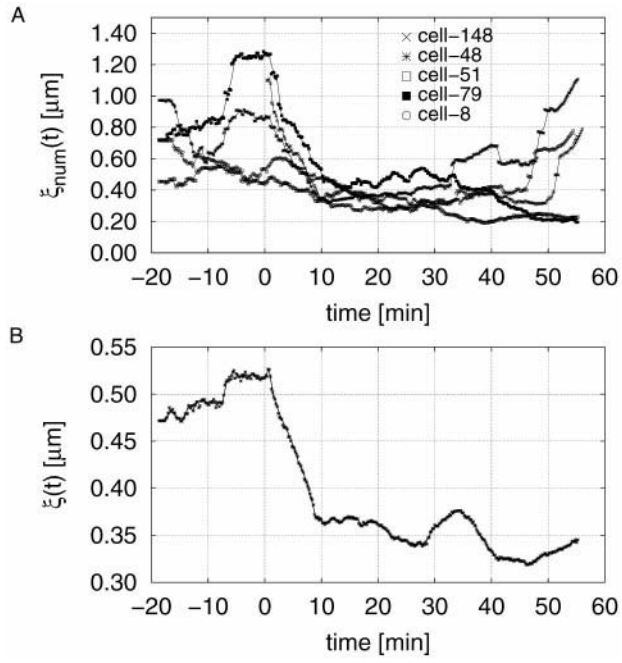

FIGURE 8 Spatial fluctuations. (*A*) Change of individual spatial fluctuations ξ as a function of time for the same cells as in Figs. 5–6. After the onset of shear stress at time $t = 0$ min (50 dyn/cm^2), the spatial fluctuations around the mean trajectories are clearly reduced. (*B*) The same phenomena as average value over all cell paths displayed in Fig. 5 *A*.

Alignment in the direction of flow

Analyses of cell alignment in fluid shear stress were performed for individual cells and for cell ensembles of confluent monolayers. The orientations $\varphi(t) \in [0, 180^o]$ (measured with respect to the x-axis) of individual cells displayed the heterogeneous behavior as seen for motility parameters. As shown in Fig. 9, cell 8 slowly but continuously orients toward the direction of flow (~123°), whereas cells 51 and 48 display large variations but finally tend to align. In contrast, cells 148 and 79 seem to be unrelated to shear stress. It is remarkable that the orientation of cells changes even without shear stress.

Mean values of alignment were determined and quantified as follows. The absolute orientation $\varphi_i \in [0, 180^o]$ of each cell, which is available from image segmentation, can be transformed to a relative orientation $\phi_i \in [-90, +90^o]$ with respect to the direction of shear stress θ. The value $\phi_i = 0$ corresponds to an orientation parallel to the direction of shear stress. The standard deviation $\sigma(t)$ delivers a collective measure characterizing the orientation of all cells with respect to the direction of shear stress θ. $\sigma(t)$ is defined as

$$\sigma^2(t) = \frac{1}{N}\sum_{i=1}^{N}[\phi_i(t)]^2$$

with $N = N(t)$ as the number of cells at time step t. Whereas $\sigma(t)$ takes the value of $\pi/(2 \cdot 3^{1/2})$ (corresponding to ~52°) for a completely random oriented system, $\sigma(t)$ tends to lower values for cells that align parallel to the direction of shear stress θ. If the number of cells with orientations between ϕ and $\phi + \delta\phi$ is plotted in a histogram, the mean alignment process can be observed by a bell-shaped curve around $\phi = 0$, where $\sigma(t)$ represents the extension of this bell-like curve. Thus, application of shear stress results in a peaked curve for cells that are going to align with the direction of flow.

In a further study we examined the responses of different levels of shear stress simultaneously in four rheological units by the use of the fully automated setup. Four points were selected within each unit and repeatedly automatically analyzed. Cells clearly respond to high shear stress, and the effects are less significant at low shear stress values (Fig. 10).

Structure index

Besides the change of orientation, shear stress also changes the shape of cells, which can be quantified with a structure index. The time-dependent mean structure index $\langle SI(t)\rangle$ is defined as

$$\langle SI(t)\rangle = \frac{1}{N}\sum_{i=1}^{N}\frac{4\pi A_i(t)}{P_i^2(t)}$$

in which A_i represents the cell area, P_i the cell perimeter, and $N = N(t)$ the number of cells at time t. Therefore, the structure index is directly available from image segmentation. The structure index is 1 for circular objects and tends

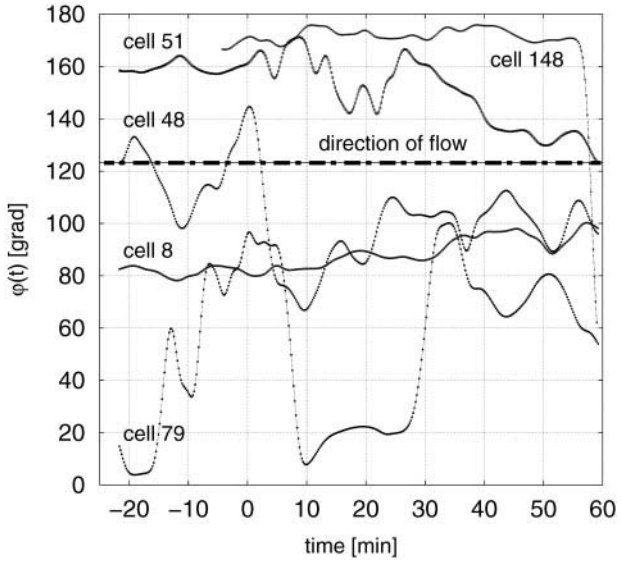

FIGURE 9 Individual cell orientations as a function of time. Cell orientation $\varphi(t)$ is measured with respect to the x-axis. At time $t = 0$ min shear stress of 50 dyn/cm^2 is applied. The direction of shear stress is indicated by a straight line at 123° (compare Fig. 5). Cells even change orientation without shear stress and respond to shear stress individually and heterogeneously. Whereas cell 8 aligns rather continuously to the direction of flow, other cells even rotate against the direction of flow. Remarkably, cells even change their orientation under resting conditions.

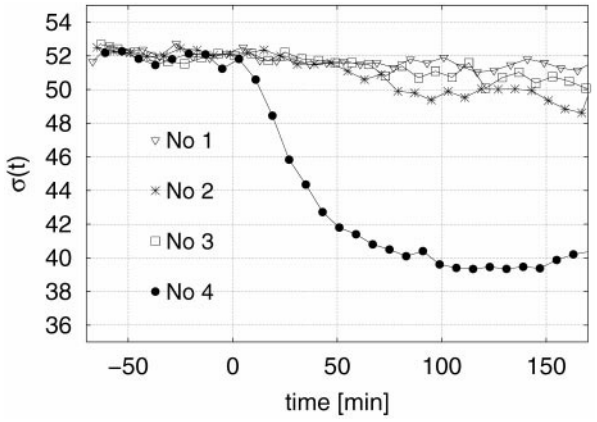

FIGURE 10 Mean orientations of shear stress exposed endothelial cells. The decrease of the mean orientation described by parameter $\sigma(t)$ was examined within one experiment (4 heads each with 4 measurement points) under different levels of shear stress. Thus, ~1000 cells are observed within one head. Numbers 1–4 denote individual units with different shear stress values: 0 dyn/cm^2 in 1, 6 dyn/cm^2 in 2, 12 dyn/cm^2 in 3, and 68 dyn/cm^2 in 4. Time point $t = 0$ min indicates onset of shear stress. Whereas shear stress levels of 12 dyn/cm^2 and below had only less effect on orientation, cells responded to 68 dyn/cm^2 within 10 min.

toward zero for elongated (cigar-like) forms. An example of SI behavior is discussed below (see Fig. 11).

Time course of cell motility, alignment, and elongation of endothelial cells in fluid shear stress

So far, experiments showed that endothelial cells respond to shear stress by a staggered change of migration activity, alignment, and structure index. Although cell cultures of different isolates showed heterogeneity, in the time-related response all experiments showed a sequential time course composed in the sequence of change in migration activity, alignment, and elongation. Based on these observations we propose a sequential activation of mechanisms responsible for the change in each parameter. Thus, we classified the onset of each parameter as a beginning of a characteristic phase.

As shown in Fig. 11, in phase I, under resting conditions, all mean parameters remain constant apart from small variations around their mean values. After the onset of shear stress the cell motility changes markedly (phase II), whereas the orientation remains constant over a period of time and seems to depend on the level of shear stress. Phase III begins with a clear alignment characterized by $\sigma(t)$. Commonly, the change of structure index also shows a delay, and is maintained in the order of hours. As seen in Fig. 11, in relation to shear stress applied, change of the structure index (phase IV) occurred with a lag period that was much longer than the change of σ as a parameter for cell alignment.

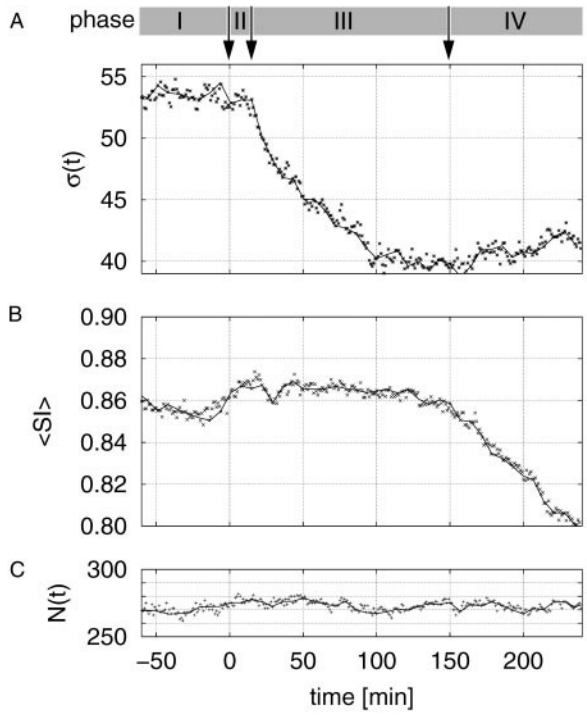

FIGURE 11 Phase behavior of shear stress-exposed endothelial cells. The response of endothelial cells to shear stress can be classified in several phases. Under resting conditions (phase I), the mean orientation parameter $\sigma(t)$ (*A*), the mean structure index $\langle SI \rangle$ (*B*), and the cell number N of the observed region (*C*) remain constant. After the onset of shear stress at time $t = 0$ min (25 dyn/cm^2), $\sigma(t)$ does not change (phase II). This happens with a delay of ~10–20 min (phase III). Finally, the mean structure index decreases (phase IV) indicating a change to a more elongated cell structures.

DISCUSSION

The setup

In the present work we describe an improved rheological in vitro system and novel software that allow a detailed analysis of cellular responses to fluid shear stress on the base of morphodynamical changes in subconfluent and confluent cell cultures. Furthermore, automation of both data acquisition and data analysis allow handling of large data sets at the same time period for up to 12 individual units and in high time resolution. The system is equipped with precise positioning stages (rotation of the revolver plate and the microscope) that allow repeated refinding of cell areas with a precision of 16 μm at the rotary stage and 1 μm at the linear stage. Thus, lenses up to 100× can be used to repeatedly investigate the very same cells, including subcellular effects.

The stable mechanical setup of the rheometer system provides the basis of the image processing analysis and the further calculation of parameters. Whereas the mathematical parameters are exactly defined, they are influenced both from measurement errors, e.g., finite pixel resolution or microscopic and camera aberrations, and real intrinsic dynamical processes. Thus, variation of parameters as function of time without external shear stress, as for example the nonconstant value of $\sigma(t)$ in phase I displayed in Fig. 11, might be caused by both influences. However, Fig. 9, which represents individual cell orientations as a function of time, shows that there is a differentiated behavior of living cells in confluent cultures that is able to cause fluctuations of mean parameters even under constant external conditions.

In this context, statistics plays a major role in the calculation of mean values. As calculated for an infinite large and random oriented system, the value of σ is 51.9615°. The experiment in Fig. 11 (phase I) displays a value of ~53.5°, whereas the experiment in Fig. 10 delivers a value of ~52° under resting conditions. Now, the calculation of the variance of σ as function of the system size N gives values of $\pm 1.5°$ for $N = 270$ (corresponding to Fig. 11) and of $\pm 0.7°$ for $N = 1000$ (corresponding to Fig. 10). Thus, cells of Fig. 11 do not necessarily prefer a special orientation under resting conditions, because the deviation of σ is within the statistical variations of an ensemble of $N = 270$ cells.

Finally, it is important to check the quality of the image processing analysis. Because the distance covered by cells

in confluent culture is lower and much more localized than for single cells, we have checked to determine whether it is possible to distinguish the spatial fluctuations of trajectories of fixed and living cells. We found within a control experiment that living cells showed fluctuations that are factors 2–3 times as large as those of fixed cells. The spatial fluctuations of fixed cells, which should ideally be zero, took a value slightly about the theoretical value of 0.1 μm based on an inspection of the finite pixel resolution. Thus, above this limit it is even possible to quantitatively uncover shear stress-induced effects on cultured cells even at confluency.

Apart from investigation of physiological effects on endothelial cells, shear stress has been described to serve as a load test in cell biology research, especially to quantify cell-to-cell and cell-to-substrate adhesion and to uncover drug-induced effects on culture cells. For such an application the developed setup might also provide a valuable tool (Schnittler et al., 1993, 1997; Schnittler, 1998; Yap et al., 1997, 1998; Wechezak et al., 1989).

Endothelial cell cultures display a characteristic phase behavior in adaptation to fluid shear stress

As an application of the designed setup we first analyzed shear stress-induced morphodynamic changes of cultured endothelial cells by high time resolution. Comparing the values of cell motility, degree of alignment, and change in the structure index, we could show that confluent cultures of porcine endothelial cells respond to shear stress with a characteristic phase behavior of the following time course: resting conditions (phase I), change of cell motility (phase II), onset of alignment (phase III), and finally cell elongation (phase IV). This phase behavior was observed in every experiment. Whereas the shear stress-induced morphodynamic parameters showed a time and dose dependency of comparable values when cells of the same isolates were examined, cells of different isolates displayed differences with respect to the onset of each phase. In addition, parameters of different cell isolates under resting culture conditions displayed this heterogeneity as well. We first assumed that slight variations of cell density might be responsible, but correlation of the parameters with respect to cell density was only very rough (data not shown) not valid to explain the observed differences. Thus, we assume that the heterogeneous behavior under resting and shear stress conditions is primarily based on different features of the cultures isolated from different pig pulmonary trunk vessels. It is well known that isolates of the same cell type display variable growth and other characteristics, such as the degree of autocrine activity (Battistini et al., 1993; Aitkenhead et al., 1998; Kozian et al., 1997; Taylor and Alexander, 1993; Lopez-Farre et al., 1997) that in turn will influence the cell-to-cell and cell-to-substrate adhesion. This could explain the observed heterogeneity between different cultures. Failures of the geometry of the individual heads can be excluded because the precision of the shear space is extremely high and the asymmetry of the cone in relation to the plate is $<1\%$ (Schnittler et al., 1993). In addition, we have used the same cones for different cell cultures, and vice versa. All experiments lead to the same results as between different cones and units (data not shown).

Individual cells within confluent monolayers display heterogeneous morphodynamics

Tracing of individual cell paths also displayed a heterogeneous quantitative behavior with respect to morphodynamic parameters. This heterogeneity of cells within confluent cultures has not been described in detail and the molecular mechanisms are still unclear. It can be assumed that cell culture conditions and the stage of cell cycle even at comparable cell density leading to different local environments might contribute to heterogeneity. Another possibility for heterogeneity might arise from local topographical differences at the surface between individual cells (for review see Davies et al., 1999). Otherwise, heterogeneity was also observed under resting culture conditions. A further point is the communication and interaction of cells mediated by cell-to-cell junctions and cell-to-substrate adhesion contributing to the individual behavior of the cells under resting and shear stress conditions (discussed below).

Shear stress causes an initial reduction of fluctuations and increased locomotion velocity (phase II)

The first observable shear stress-induced effect on endothelial cells was the inhibition of zigzag movements (e.g., spatial fluctuations around mean cell trajectories) that happened within minutes after the onset of flow. It is rather unlikely that this phenomenon is caused by simple mechanical alterations, such as pressing the cells against the substrate. We rather assume a shear stress-induced activation of cell-to-substrate and cell-to-cell junctions that both might inhibit the mean fluctuations of the cells and promote a directed cell movement observed after onset of shear stress. This assumption is further supported by the observation that shear stress causes a remodeling of focal adhesion sites (Davies et al., 1994) and activation of focal adhesion kinases (FAK) within a minute (Li et al., 1997). Integrin activation has been suggested to increase the binding strength of integrin-receptors to their ligands, but also promotes migration activity (LaFlamme et al., 1994; Imhof et al., 1997; Yamada, 1997; Akiyama et al., 1994). The activation of heterodimeric integrin subsets might contribute to the two different motility parameters observed (inhibition of zigzag movements and increase in directional locomotion). Furthermore, differences in adhesion strength of individual

cells within a monolayer might significantly influence the motile heterogeneity. This is supported by the observations that cell motility in particular depends on the adhesive strength of the cells to the substrate, by which intermediate strength promotes maximal migration velocity, and requires cytoskeletal-generated forces that lead to locomotion via specific integrin receptors (Lauffenburger and Horwitz, 1996; Cox and Huttenlocher, 1998; Sheetz et al., 1998, 1999). The quick response of cells to shear stress probably causes persistence of effects beyond shear stress cessation. This seems to be supported by the observation that a second onset of shear stress causes a diminished increase of locomotion velocity and in part the direction of cell locomotion, as shown in Fig. 7. This reduced response might be due to shear stress-induced adaptation that was not completely recovered after shear stress cessation within 60 min.

The role of cell-to-cell junctions in shear stress-induced cell motility, alignment, and elongation has not been addressed yet. Shear stress-induced shape change and alignment of a cell within a confluent culture also require a fine regulation of cell-to-cell junctions. We never observed formation of intercellular gaps under shear stress, even up to peak levels of 100 dyn/cm^2. Thus, a sophisticated regulation of cell-to-cell junctions must take place allowing relative movement of adjacent cells relative to each other. Moreover, a cell within a confluent monolayer is typically surrounded by other cells that do not move coordinated under resting and shear stress conditions. Therefore, it seems to be obvious that cell-to-cell junctions of one individual cell must be differentially regulated at junction-subdomains that each connect the respective cell to another adjacent cell. Such a subcellular regulation is required to maintain cell monolayer integrity, but must also allow cell motility. Morphological observations indicated that tyrosine kinase, but not protein kinase C, inhibitors are able to markedly inhibit shear stress-induced alignment and shape change (Malek and Izumo, 1996). Because various components of the endothelial cell-to-cell junctions are tyrosine kinase substrates, it is reasonable to assume that tyrosine kinase inhibition will also inhibit cell-to-cell junction reorganization that in turn might inhibit cell motility, alignment, and elongation. Recently, an interplay between N-cadherin and ectopically expressed integrins in myoblast have been shown to be required to regulate cell migration activity (Huttenlocher et al., 1998). Such a coordinated interplay between integrins and cell-to-cell junction proteins might also be important in confluent endothelial cell cultures responding to shear stress.

Alignment is not directly associated with shape change

The correlation of alignment and shape change (mean values) also shows a lack period between the onset of alignment (phase III) and the onset of shape change (phase IV) in confluent endothelial cells (Fig. 11). These data support the concept that alignment and shape change are largely independently regulated in confluent endothelial cells. The delay time between alignment and shape change proves this concept. Alignment is shear stress-dependent and seems to be primarily based on a repositioning of the cell-nucleus and the surrounding cell organelles. A shear stress-induced repositioning of the microtubule organizing center (MTOC) and GA has been shown in individual (not confluent) endothelial cells within the first hours. MTOC/GA was localized upstream according to flow direction, but randomized following longer shear stress exposure (Coan et al., 1993). The randomization of MOTC/GA after prolonged flow exposure in individual endothelial cells might be related to a missing interendothelial adhesion that further stabilizes and determines the upstream-downstream orientation of shear stress-exposed endothelial cells. In addition, it is not known whether a previous alignment is required to induce endothelial shape change. This has to be investigated further.

Phase IV was defined by the beginning of the change of structure index. Although reorientation and the process of endothelial alignment persisted in phase IV, change of structure index is based on cell elongation and typically occurred later than alignment. The separate cell elongation was characterized by plasma membrane protrusions in the long axis of the cells in both directions (in and against the flow). This conclusion is drawn from the fact that the cell nucleus and the surrounding organelles are continuously present within the center of the cells.

Based on these observations we propose that cultured endothelial adaptation to fluid flow follows a characteristic phase behavior that is largely dependent on the level of shear stress applied. Importantly, this phase behavior requires a subcellular regulation; namely, the more or less rigid rotation of the cells and/or cell organelles (reorientation) followed by a cell elongation. The activation of cell-to-cell junctions and differentiated activation of cell-to-substrate activation might significantly contribute to shear stress-induced morphodynamics and heterogeneity.

Toward a biophysical model

The present work has observed a complex and differentiated dynamical behavior of confluent cell cultures. We have found different collective phases and spatial and temporal variations of individual morphodynamic cell properties, even under resting conditions. Both are signatures of highly correlated, unstationary dynamical systems (Stanley et al., 1999; Frauenfelder et al., 1999).

To gain a deeper understanding of these phenomena it is, in our opinion, necessary to relate key components of the cell monolayer to each other within the framework of a mathematical model. Such key components could be extracted by molecular biological techniques, e.g., expressing specific receptors, combined with a detailed analysis of the

resulting morphodynamic properties that can be realized with our current system and software techniques.

Concerning cell migration, many sophisticated works have succeeded in presenting a model-based analysis of single cells (Palecek et al., 1999; Alt and Dembo, 1999; Albersdorfer et al., 1997; Kuo et al., 1997). However, the coupling of endothelial cells within confluent cultures seems to be essential to understand the dynamics and adaptation under shear stress. It is therefore necessary to construct a biophysical model that captures the interaction of cell-to-substrate and cell-to-cell adhesion together with shear stress-induced modifications of internal cell components and processes.

We thank Anne Horstkötter and Heinrich Rogge for technical assistance. The support of MOS-Technology, Warendorf, Germany; Egon Rüschenbaum Company, Vosswinkel, Germany; and Carl Zeiss Company, Jena, Germany is greatly acknowledged.

This work was supported by DFG Grants SCHN/2-1 and SCHN/1-1.

REFERENCES

Aitkenhead, M., B. Christ, A. Eichmann, M. Feucht, D. J. Wilson, and J. Wilting. 1998. Paracrine and autocrine regulation of vascular endothelial growth factor during tissue differentiation in the quail. *Dev. Dyn.* 212: 1–13.

Akiyama, S. K., S. S. Yamada, K. M. Yamada, and S. E. LaFlamme. 1994. Transmembrane signal transduction by integrin cytoplasmic domains expressed in single-subunit chimeras. *J. Biol. Chem.* 269:15961–15964.

Albersdorfer, A., T. Feder, and E. Sackmann. 1997. Adhesion-induced domain formation by interplay of long-range repulsion and short-range attraction force: a model membrane study. *Biophys. J.* 73:245–257.

Al-Mehdi, A. B., G. Zhao, and A. B. Fisher. 1998. ATP-independent membrane depolarization with ischemia in the oxygen-ventilated isolated rat lung. *Am. J. Respir. Cell Mol. Biol.* 18:653–661.

Alt, W., and M. Dembo. 1999. Cytoplasm dynamics and cell motion: two-phase flow models. *Math. Biosci.* 156:207–228.

Ando, J., and A. Kamiya. 1996. Flow-dependent regulation of gene expression in vascular endothelial cells. *Jpn. Heart J.* 37:19–32.

Ando, J., H. Nomura, and A. Kamiya. 1987. The effect of fluid shear stress on the migration and proliferation of cultured endothelial cells. *Microvasc. Res.* 33:62–70.

Asthagiri, A. R., C. M. Nelson, A. F. Horwitz, and D. A. Lauffenburger. 1999. Quantitative relationship among integrin-ligand binding, adhesion, and signaling via focal adhesion kinase and extracellular signal-regulated kinase 2. *J. Biol. Chem.* 274:27119–27127.

Battistini, B., P. Chailler, P. D'Orleans-Juste, N. Briere, and P. Sirois. 1993. Growth regulatory properties of endothelins. *Peptides.* 14: 385–399.

Birk-Sorensen, L., C. L. Kerrigan, and G. S. Jensen. 1998. E-selectin and L-selectin blockade in pure skin flaps exposed to ischemia and reperfusion injury. *Scand. J. Plast. Reconstr. Surg. Hand Surg.* 32:365–371.

Busse, R., and I. Fleming. 1995. Regulation and functional consequences of endothelial nitric oxide formation. *Ann. Med.* 27:331–340.

Coan, D. E., A. R. Wechezak, R. F. Viggers, and L. R. Sauvage. 1993. Effect of shear stress upon localization of the Golgi apparatus and microtubule organizing center in isolated cultured endothelial cells. *J. Cell Sci.* 104:1145–1153.

Cox, E. A., and A. Huttenlocher. 1998. Regulation of integrin-mediated adhesion during cell migration. *Microsc. Res. Tech.* 43:412–419.

Davies, P. F. 1991. Mechanical sensing mechanisms: shear stress and endothelial cells. *J. Vasc. Surg.* 13:729–731.

Davies, P. F. 1995. Flow-mediated endothelial mechanotransduction. *Physiol. Rev.* 75:519–560.

Davies, P. F. 1997. Overview: temporal and spatial relationships in shear stress-mediated endothelial signaling. *J. Vasc. Res.* 34:208–211.

Davies, P. F., D. C. Polacek, J. S. Handen, B. P. Helmke, and N. DePaola. 1999. A spatial approach to transcriptional profiling: mechanotransduction and the focal origin of atherosclerosis. *Trends Biotechnol.* 17: 347–351.

Davies, P. F., A. Remuzzi, E. J. Gordon, C. F. Dewey, Jr., and M. A. Gimbrone, Jr. 1986. Turbulent fluid shear stress induces vascular endothelial cell turnover in vitro. *Proc. Natl. Acad. Sci. U.S.A.* 83: 2114–2117.

Davies, P. F., A. Robotewskyj, and M. L. Griem. 1994. Quantitative studies of endothelial cell adhesion. Directional remodeling of focal adhesion sites in response to flow forces. *J. Clin. Invest.* 93:2031–2038.

Davies, P. F., A. Robotewskyj, M. L. Griem, R. O. Dull, and D. C. Polacek. 1992. Hemodynamic forces and vascular cell communication in arteries. *Arch. Pathol. Lab. Med.* 116:1301–1306.

Dewey, C. F., Jr., S. R. Bussolari, M. A. Gimbrone, Jr., and P. F. Davies. 1981. The dynamic response of vascular endothelial cells to fluid shear stress. *J. Biomech. Eng.* 103:177–185.

Dimmeler, S., J. Haendeler, V. Rippmann, M. Nehls, and A. M. Zeiher. 1996. Shear stress inhibits apoptosis of human endothelial cells. *FEBS Lett.* 399:71–74.

Dormandy, J. A. 1996. Influence of blood cells and blood flow on venous endothelium. *Int. Angiol.* 15:119–123.

Eskin, S. G., C. L. Ives, L. V. McIntire, and L. T. Navarro. 1984. Response of cultured endothelial cells to steady flow. *Microvasc. Res.* 28:87–94.

Franke, R. P., R. Fuhrmann, H. J. Schnittler, W. Petrow, and G. Simons. 1988. Human endothelial cells in vitro under a hydrodynamic shear stress: drug effects on cell adhesiveness and non-thrombogenicity of vessel intimal cells. *Vasa Suppl.* 24:11–16.

Franke, R. P., M. Grafe, H. Schnittler, D. Seiffge, C. Mittermayer, and D. Drenckhahn. 1984. Induction of human vascular endothelial stress fibres by fluid shear stress. *Nature.* 307:648–649.

Frauenfelder, H., P. G. Wolynes, and R. H. Austin. 1999. Biological physics. *Rev. Mod. Phys.* 71.

Girard, P. R., and R. M. Nerem. 1993. Endothelial cell signaling and cytoskeletal changes in response to shear stress. *Front. Med. Biol. Eng.* 5:31–36.

Gonzalez, E. R., and B. S. Kannewurf. 1998. Atherosclerosis: a unifying disorder with diverse manifestations. *Am. J. Health Syst. Pharm.* 55: S4–S7.

Hudlicka, O. 1998. Is physiological angiogenesis in skeletal muscle regulated by changes in microcirculation? *Microcirculation.* 5:5–23.

Huttenlocher, A., M. Lakonishok, M. Kinder, S. Wu, T. Truong, K. A. Knudsen, and A. F. Horwitz. 1998. Integrin and cadherin synergy regulates contact inhibition of migration and motile activity. *J. Cell Biol.* 141:515–526.

Huttenlocher, A., R. R. Sandborg, and A. F. Horwitz. 1995. Adhesion in cell migration. *Curr. Opin. Cell Biol.* 7:697–706.

Imhof, B. A., D. Weerasinghe, E. J. Brown, F. P. Lindberg, P. Hammel, L. Piali, M. Dessing, and R. Gisler. 1997. Cross talk between alpha(v)beta3 and alpha4beta1 integrins regulates lymphocyte migration on vascular cell adhesion molecule 1. *Eur. J. Immunol.* 27:3242–3252.

Kozian, D. H., M. Ziche, and H. G. Augustin. 1997. The activin-binding protein follistatin regulates autocrine endothelial cell activity and induces angiogenesis. *Lab. Invest.* 76:267–276.

Kuo, S. C., D. A. Hammer, and D. A. Lauffenburger. 1997. Simulation of detachment of specifically bound particles from surfaces by shear flow. *Biophys. J.* 73:517–531.

LaFlamme, S. E., L. A. Thomas, S. S. Yamada, and K. M. Yamada. 1994. Single subunit chimeric integrins as mimics and inhibitors of endogenous integrin functions in receptor localization, cell spreading and migration, and matrix assembly. *J. Cell Biol.* 126:1287–1298.

Langille, B. L., and S. L. Adamson. 1981. Relationship between blood flow direction and endothelial cell orientation at arterial branch sites in rabbits and mice. *Circ. Res.* 48:481–488.

Lauffenburger, D. A., and A. F. Horwitz. 1996. Cell migration: a physically integrated molecular process. *Cell.* 84:359–369.

Li, S., M. Kim, Y. L. Hu, S. Jalali, D. D. Schlaepfer, T. Hunter, S. Chien, and J. Y. Shyy. 1997. Fluid shear stress activation of focal adhesion kinase. Linking to mitogen-activated protein kinases. *J. Biol. Chem.* 272:30455–30462.

Lopez-Farre, A., L. Sanchez de Miguel, C. Caramelo, J. Gomez-Macias, R. Garcia, J. R. Mosquera, T. de Frutos, I. Millas, F. Rivas, G. Echezarreta, and S. Casado. 1997. Role of nitric oxide in autocrine control of growth and apoptosis of endothelial cells. *Am. J. Physiol.* 272:H760–H768.

Malek, A. M., and S. Izumo. 1995. Control of endothelial cell gene expression by flow. *J. Biomech.* 28:1515–1528.

Malek, A. M., and S. Izumo. 1996. Mechanism of endothelial cell shape change and cytoskeletal remodeling in response to fluid shear stress. *J. Cell Sci.* 109:713–726.

Nerem, R. M. 1993. Hemodynamics and the vascular endothelium. *J. Biomech. Eng.* 115:510–514.

Niebauer, J., and J. P. Cooke. 1996. Cardiovascular effects of exercise: role of endothelial shear stress. *J. Am. Coll. Cardiol.* 28:1652–1660.

Nilius, B., F. Viana, and G. Droogmans. 1997. Ion channels in vascular endothelium. *Annu. Rev. Physiol.* 59:145–170.

Palecek, S. P., A. F. Horwitz, and D. A. Lauffenburger. 1999. Kinetic model for integrin-mediated adhesion release during cell migration. *Ann. Biomed. Eng.* 27:219–235.

Palecek, S. P., A. Huttenlocher, A. F. Horwitz, and D. A. Lauffenburger. 1998. Physical and biochemical regulation of integrin release during rear detachment of migrating cells. *J. Cell Sci.* 111:929–940.

Papadaki, M., and S. G. Eskin. 1997. Effects of fluid shear stress on gene regulation of vascular cells. *Biotechnol. Prog.* 13:209–221.

Roca, J., T. P. Gavin, M. Jordan, N. Siafakas, H. Wagner, H. Benoit, E. Breen, and P. D. Wagner. 1998. Angiogenic growth factor mRNA responses to passive and contraction-induced hyperperfusion in skeletal muscle. *J. Appl. Physiol.* 85:1142–1149.

Russ, J. C. 1999. The image processing handbook. CRC Press.

Sastry, S. K., M. Lakonishok, S. Wu, T. Q. Truong, A. Huttenlocher, C. E. Turner, and A. F. Horwitz. 1999. Quantitative changes in integrin and focal adhesion signaling regulate myoblast cell cycle withdrawal. *J. Cell Biol.* 144:1295–1309.

Sato, Y., K. Tsukada, and K. Hatakeyama. 1999. Role of shear stress and immune responses in liver regeneration after a partial hepatectomy. *Surg. Today.* 29:1–9.

Schnittler, H. J. 1998. Structural and functional aspects of intercellular junctions in vascular endothelium. *Basic Res. Cardiol.* 93:30–39.

Schnittler, H. J., R. P. Franke, U. Akbay, C. Mrowietz, and D. Drenckhahn. 1993. Improved in vitro rheological system for studying the effect of fluid shear stress on cultured cells. *Am. J. Physiol.* 265:C289–C298.

Schnittler, H. J., B. Puschel, and D. Drenckhahn. 1997. Role of cadherins and plakoglobin in interendothelial adhesion under resting conditions and shear stress. *Am. J. Physiol.* 273:H2396–H2405.

Schnittler, H. J., A. Wilke, T. Gress, N. Suttorp, and D. Drenckhahn. 1990. Role of actin and myosin in the control of paracellular permeability in pig, rat and human vascular endothelium. *J. Physiol. (Lond.).* 431: 379–401.

Sheetz, M. P., D. P. Felsenfeld, and C. G. Galbraith. 1998. Cell migration: regulation of force on extracellular-matrix-integrin complexes. *Trends Cell Biol.* 8:51–54.

Sheetz, M. P., D. Felsenfeld, C. G. Galbraith, and D. Choquet. 1999. Cell migration as a five-step cycle. *Biochem. Soc. Symp.* 65:233–243.

Skalak, T. C., and R. J. Price. 1996. The role of mechanical stresses in microvascular remodeling. *Microcirculation.* 3:143–165.

Soler, H. M., M. T. Watkins, H. Albadawi, H. Kadowaki, and G. M. Patton. 1997. Effects of oxygen tension and shear stress on human endothelial cell prostacyclin production. *J. Surg. Res.* 67:46–53.

Stanley, H. E., L. A. N. Amaral, A. L. Goldberger, S. Havlin, P. Ch. Ivanov, and C.-K. Peng. 1999. Statistical physics and physiology: monofractal and multifractal approaches. *Physica A.* 270:309–324.

Takahashi, M., T. Ishida, O. Traub, M. A. Corson, and B. C. Berk. 1997. Mechanotransduction in endothelial cells: temporal signaling events in response to shear stress. *J. Vasc. Res.* 34:212–219.

Tardy, Y., N. Resnick, T. Nagel, M. A. Gimbrone, Jr., and C. F. Dewey, Jr. 1997. Shear stress gradients remodel endothelial monolayers in vitro via a cell proliferation-migration-loss cycle. *Arterioscler. Thromb. Vasc. Biol.* 17:3102–3106.

Taylor, W. R., and R. W. Alexander. 1993. Autocrine control of wound repair by insulin-like growth factor I in cultured endothelial cells. *Am. J. Physiol.* 265:C801–C805.

Traub, O., and B. C. Berk. 1998. Laminar shear stress: mechanisms by which endothelial cells transduce an atheroprotective force. *Arterioscler. Thromb. Vasc. Biol.* 18:677–685.

Ueba, H., M. Kawakami, and T. Yaginuma. 1997. Shear stress as an inhibitor of vascular smooth muscle cell proliferation. Role of transforming growth factor-beta 1 and tissue-type plasminogen activator. *Arterioscler. Thromb. Vasc. Biol.* 17:1512–1516.

Wechezak, A. R., D. E. Coan, R. F. Viggers, and L. R. Sauvage. 1993. Dextran increases survival of subconfluent endothelial cells exposed to shear stress. *Am. J. Physiol.* 264:H520–H525.

Wechezak, A. R., T. N. Wight, R. F. Viggers, and L. R. Sauvage. 1989. Endothelial adherence under shear stress is dependent upon microfilament reorganization. *J. Cell Physiol.* 139:136–146.

Yamada, K. M. 1997. Integrin signaling. *Matrix Biol.* 16:137–141.

Yap, A. S., W. M. Brieher, M. Pruschy, and B. M. Gumbiner. 1997. Lateral clustering of the adhesive ectodomain: a fundamental determinant of cadherin function. *Curr. Biol.* 7:308–315.

Yap, A. S., C. M. Niessen, and B. M. Gumbiner. 1998. The juxtamembrane region of the cadherin cytoplasmic tail supports lateral clustering, adhesive strengthening, and interaction with p120ctn. *J. Cell Biol.* 141: 779–789.